

4-2023

Feasibility analysis of a wave powered autonomous underwater vehicle

Yingchen Yang

The University of Texas Rio Grande Valley, yingchen.yang@utrgv.edu

Erick Martinez

The University of Texas Rio Grande Valley

Follow this and additional works at: https://scholarworks.utrgv.edu/me_fac

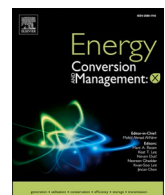
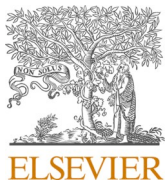


Part of the Mechanical Engineering Commons

Recommended Citation

Yang, Yingchen, and Erick Martinez. "Feasibility analysis of a wave powered autonomous underwater vehicle." Energy Conversion and Management: X 18 (2023): 100352. <https://doi.org/10.1016/j.ecmx.2023.100352>

This Article is brought to you for free and open access by the College of Engineering and Computer Science at ScholarWorks @ UTRGV. It has been accepted for inclusion in Mechanical Engineering Faculty Publications and Presentations by an authorized administrator of ScholarWorks @ UTRGV. For more information, please contact [william.flores01@utrgv.edu](mailto:wiliam.flores01@utrgv.edu).



Feasibility analysis of a wave powered autonomous underwater vehicle

Yingchen Yang^{*}, Erick Martinez

Department of Mechanical Engineering, University of Texas Rio Grande Valley, Edinburg, TX 78539, USA



ARTICLE INFO

Keywords:

Autonomous underwater vehicle
AUV
Wave energy converter
WEC
Mass-spring-damper
Non-resonant

ABSTRACT

An autonomous underwater vehicle (AUV) powered by renewable energy would enable it to extend endurance and forward presence with no logistics tail for fuel. A wave powered concept AUV is proposed and analyzed for this purpose. The AUV is in a torpedo shape and employs a fully hull-encapsulated mass-spring-damper system as its power take-off (PTO) unit. While in the recharging mode, the AUV surfaces and converts wave energy for electricity. Considering the AUV of a common size, our analysis indicates that resonance of the AUV and/or its PTO, to be excited by ocean waves, becomes impossible in typical ocean conditions. Then by making the AUV almost fully submerged to eliminate its intrinsic resonant nature and by applying some realistic constraints, the AUV's power generation capability without resonance is characterized. Our simulation results show that the AUV is still capable of generating power at a decent level in a wide range of the wave frequency upon optimization. Some guiding principles have been established for AUV design of this type.

1. Introduction

An autonomous underwater vehicle (AUV) is an unmanned underwater robot capable of completing pre-programmed missions with little or no human interaction. AUVs have a wide range of applications in scientific explorations (e.g., ocean surveying, pollution tracing, etc.), industrial practices (e.g., fishery, undersea cable and pipeline inspection, etc.), and military operations (e.g., undersea surveillance, reconnaissance, etc.) [1]. Due to the strong market demand, more than 100 makes/models of AUVs have been developed worldwide [2]. A major issue is that the existing AUVs are mostly powered by batteries and have a measured endurance in hours or days per battery charge [3]. They need periodical recharging and redeployment from a dedicated host platform or support vessel, which is often expensive and inconvenient. By making an AUV harvest energy from the environment and become self-rechargeable, it can easily increase the endurance to months or longer.

A very limited number of self-recharging AUVs have been explored by researchers so far [4]. In utilizing solar energy, SAUV-II [5] is one among others. Due to the limited sunlight availability and its low power density, however, SAUV-II has to spend all the daylight time for recharging and only the nighttime for missions. Biofouling also largely affects the SAUV-II recharging. In using ocean temperature gradients, SOLO-TREC demonstrated the first successful application in powering an underwater glider (one type of AUVs) [6], followed by some other

similar technologies [7]. But this AUV class is limited to a periodic descending-ascending forward motion at a very low speed. In using ocean waves, an AUV platform equipped with an internally placed gyroscopic wave energy converter has been investigated [3]. The in-situ testing showed a very low power generation capability though [8], making it impractical for real AUV applications. Another AUV platform equipped with an externally placed but retractable oscillating ellipsoidal hydrofoil for energy harvesting has been numerically studied [9]. Furthermore, an AUV that relies on a wave-excited rolling oscillation of the AUV body about its longitudinal axis and an internal pendulum for power take-off has been experimentally examined [10]. Some other technologies also demonstrated usage of renewable energy sources for direct surface propulsion rather than recharging a battery for underwater operation. For example, Ocean Aero developed a retractable folding windsail concept to use winds to directly propel an autonomous underwater and surface vehicle [11]. Liquid Robotics demonstrated a two-body wave glider, which uses waves for direct propulsion [12].

The ocean is a huge reservoir of renewable energy in forms of waves, tides, currents, temperature gradients, and salinity gradients. Among them, waves have the best potential for energy harvesting due to their high power density and unlimited site availability [13]. In comparison with sunlight and winds, ocean waves offer about an order of magnitude higher power density [14] and an almost 24/7/365 energy flux consistency [15]. The high power density of waves permits a small size and high output of the energy harvesting unit, which is particularly suited

* Corresponding author.

E-mail address: yingchen.yang@utrgv.edu (Y. Yang).

for a compact AUV design. The consistent energy flux of waves guarantees the AUV to have such a renewable energy source available anywhere and anytime. These two advantages make the ocean waves a great candidate to feed power to AUVs for self-recharging. Unfortunately, a successful approach of this kind is yet to be demonstrated.

Due to the advantages of waves over the other renewable energy sources to power self-recharging AUVs, and in consideration of lack of successful demonstration, both fundamental research and technological advancement along this line are much needed. In utilizing waves to generate electricity in a utility scale, a large variety of wave energy converter (WEC) technologies have been explored in recent years [16–18]. Most of them, however, are not transferable to AUV applications simply because their operation conditions are not compatible with that of AUVs. Yet, a reciprocating WEC (heaving up and down and/or swaying back and forth) in a shape of a spar buoy and with a fully hull-encapsulated mass-spring-damper system for power takeoff (PTO) deserves special attention [19–21]. It is compact, portable, and self-contained. It demonstrates an unrivaled potential for application to a wave powered AUV.

For the hull-encapsulated mass-spring-damper mechanism as a PTO, it demands the resonance of the carrying platform in waves for the best efficiency. For a WEC to be the carrying platform, the demand can be met by appropriately adjusting certain design parameters. For an AUV to be the carrying platform, however, such parametric adjustment to meet the resonance requirement becomes impossible due to some realistic constraints (see detailed discussion in Section 4). Therefore, the technology transfer from a WEC to an AUV still face challenges.

In the present research, we propose a wave powered AUV, which is in a torpedo shape and employs an embedded mass-spring-damper mechanism as its PTO. Such a wave powered AUV concept has never been reported in the literature or in the AUV industry to the best of our knowledge. The torpedo shape is the most widely adopted shape in existing AUV designs and mostly mimics a spar buoy that well suits the mass-spring-damper mechanism. Using this wave powered AUV as a model, we discuss its inability of resonance in waves, present an approach to eliminate the intrinsic resonant nature, characterize the non-resonant behavior, and estimate the power generation capability.

2. Conceptual model

Our proposed wave powered AUV concept is illustrated in Fig. 1. This self-recharging AUV is in the most popular torpedo shape and has a watertight rigid hull. Inside the hull there are a front and a rear payload bay for mission-required sensors and/or instruments, a mass-spring-

damper PTO unit in the middle, and a ballast tank as well as a propulsion unit towards the trailing end. With focus on the PTO unit for self-recharging, it comprises a spiral shaped compression spring, two disc springs, a translator, and a set of stators. When the AUV performs certain types of reciprocating motion in waves (e.g., heave, pitch, etc.), the inside translator will oscillate along a smooth guide rail assisted by the springs, and the created relative motion between the translator and the stator set leads to generation of electricity. The two high-stiffness disc springs applied to the two stroke ends provide overrange protection and enable frequency up-conversion (see detailed discussion in Section 5.1). The rechargeable battery pack, which is usually the heaviest component in AUVs, can be embedded in the translator as illustrated to increase the sliding mass for a high efficiency.

The AUV of Fig. 1 is expected to operate in two modes – underwater cruising mode to fulfil missions, and surface recharging mode by riding waves. The two modes are depicted in Fig. 2. In the cruising mode, the AUV is near to a neutral buoyancy and typically remains a horizontal orientation in an underwater environment for forward motion (Fig. 2a). In the recharging mode, however, the AUV will surface by active ballast control, and may be in one out of three typical equilibrium orientations in calm seas – horizontal (Fig. 2b), inclined (Fig. 2c), and vertical (Fig. 2d). The different equilibrium orientations can be achieved by positioning the ballast tank in different locations inside the AUV. The ballast tank location shown in Fig. 1 is to achieve a vertical equilibrium orientation.

Among the three equilibrium orientations in Fig. 2b, c, and d, the horizontal orientation requires the AUV's longitudinal axis to be aligned along the wave propagation direction. For a torpedo shaped AUV that is powered off and that freely floats on the ocean surface, however, waves

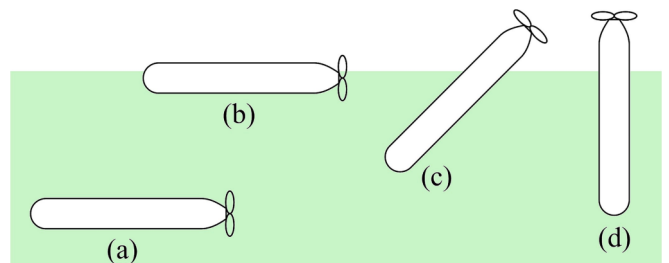


Fig. 2. Cruising mode (a) and recharging mode (b, c, or d). In the recharging mode, the surface floating AUV could be in a horizontal orientation (b), an inclined orientation (c), or a vertical orientation (d).

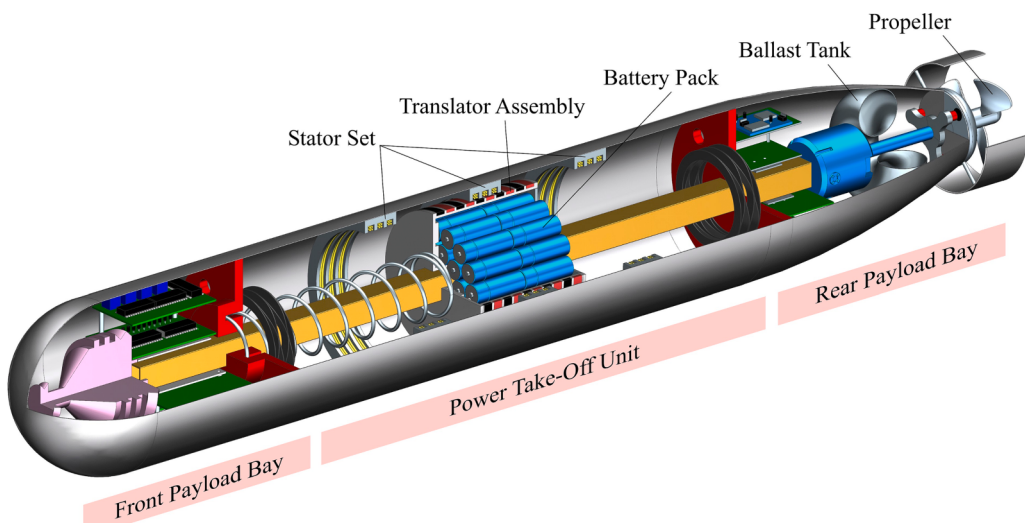


Fig. 1. Cutaway view of the wave powered AUV concept.

may not be able to automatically align it that way and maintain the orientation that way. Some hydrodynamic designs (e.g., adding a long fin) could help achieve such a passive control to meet the orientation needs, but they could also negatively affect the AUV's hydrodynamic performance in the cruising mode. In contrast, the vertical orientation (Fig. 2d) would never have such an alignment issue, and most existing AUVs would incorporate well with such an orientation without modifying their existing hydrodynamic designs. In the present work, we focus on the AUV's recharging mode and evaluate the feasibility by considering the vertical orientation only.

3. Statistical data

For development of a wave powered AUV, understanding waves and AUVs from a statistics point of view is of great importance. The statistics helps reveal potential issues and guide engineering practice.

Figs. 3 and 4 show histograms of the wave period and wave height in the Pacific Ocean and the Gulf of Mexico, respectively. Original data were obtained from the buoy station 51,000 (Pacific Ocean, 23.535 N 153.781 W) and the buoy station 42,002 (Gulf of Mexico, 26.055 N 93.646 W) maintained by NOAA National Data Buoy Center [22]. The data were analyzed on an hourly basis across three years from October 1, 2016 to September 30, 2019. As shown in Fig. 3, in the Pacific Ocean the dominant wave period occurs between 9 s and 10 s (Fig. 3a) and the dominant wave height appears between 1.6 m and 2.2 m (Fig. 3b). In comparison, in the Gulf of Mexico the dominant wave period is between 5 s and 8 s (Fig. 4a) and the dominant wave height is between 0.6 m and 1.2 m (Fig. 4b). In the present work, we take a wave period of 9.5 s and a wave height of 1.9 m to represent the most common wave conditions in the Pacific Ocean, and a wave period of 6.5 s and a wave height of 0.9 m in the Gulf of Mexico. The corresponding dominant frequencies for Pacific waves and Gulf waves are 0.105 Hz and 0.154 Hz, respectively.

Evidently, the Pacific waves possess longer periods and larger heights than the Gulf waves in general. In other words, the Pacific waves have higher power density than Gulf waves since the power density is proportional to the wave period and the wave height squared [23]. Nonetheless, in wave energy conversion, a WEC's energy harvesting capability decreases with an increasing wave period [24]. This way, waves with a shorter period (higher frequency) are more in favor of energy conversion. Therefore, the relatively low power density of the Gulf waves can be largely compensated by the relatively low wave period in energy conversion.

With AUVs in broad applications, there are more than 100 makes/models being developed worldwide [2]. Among them, a huge majority adopted a torpedo shape. Fig. 5 shows histograms of the body length L and aspect ratio σ among 87 makes/models of torpedo shaped AUVs. The original data were obtained from the database maintained by the Autonomous Undersea Vehicle Applications Center [2]. According to Fig. 5a, the most common body lengths are between 1.5 m and 2 m, about 94 % of the body lengths are below 7 m, and no body length of more than 11 m has ever been pursued. The aspect ratio σ is defined as the ratio between the body length L and the body diameter D , $\sigma = L/D$. As shown in Fig. 5b, the most common aspect ratio is between 6 and 7.

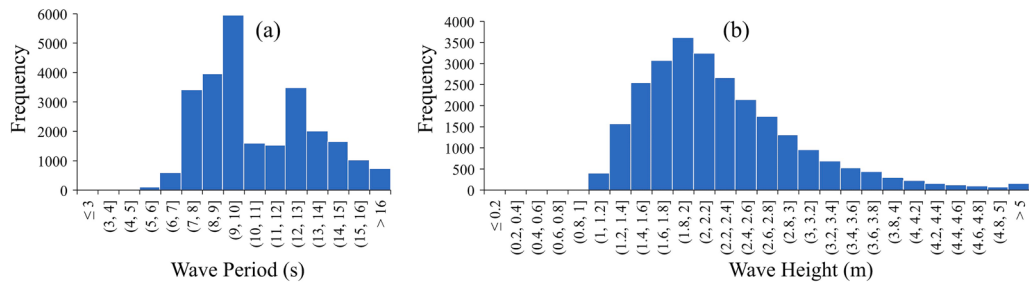


Fig. 3. Histogram of the wave period (a) and wave height (b) in the Pacific Ocean.

AUVs with an aspect ratio below 5 or above 15 become rare.

4. Resonant approach: Challenges

Wanted or not, in development of WECs that perform reciprocating motions while riding waves, the resonance principle is mostly followed [16]. When a WEC's natural frequency matches with the dominant wave frequency, resonance occurs and the WEC has a high capture width ratio (i.e., the efficiency). In the case of a mismatch, the capture width ratio becomes very low. In integrating such a WEC unit into an AUV design, the resonance principle remains effective.

A fact is that, in typical ocean conditions, the dominant wave frequency is generally low. Using the Pacific waves as an example, the most common wave frequency is $f_w = 0.105$ Hz (Fig. 3a). To make the natural frequency of a WEC match with such a low wave frequency, the WEC must be massive in terms of mass and volume [18]. Considering the best known WEC—the PB3 PowerBuoy—as an example, it weighs 8,300 kg [25]. This weight is about one to three orders of magnitude higher than that of most AUVs ever developed. Therefore, letting a light weighted AUV resonate at a typical wave frequency is very unlikely feasible. This challenge can be further revealed in relation to our proposed concept AUV (Fig. 1) by using different measures as discussed in the following.

4.1. Heave resonance

Consider the concept AUV in the vertical orientation for recharging, and assume that it is partially submerged and heaves up and down in waves with no pitch motion. As illustrated in Fig. 6, the AUV is simplified to a spar buoy with a draft d . Under such conditions, the AUV can be mathematically modelled as two mass-spring-damper subsystems that are coupled with one inside another. The outside subsystem consists of the seawater and the vertically floating AUV body. The inside one is the PTO – a spring-suspended translator with its motion being damped by the stator set when generating electricity.

Define the AUV's total mass M , the PTO's spring-suspended mass m (i.e., the translator), the AUV's heave added mass m_{add} , the AUV's vertical displacement z_{AUV} , the AUV's linearized viscous damping λ and hydrostatic heave stiffness k_{AUV} , the PTO translator's vertical displacement z_{PTO} , as well as the PTO's electromagnetic damping c_{PTO} and spring stiffness k_{PTO} . The AUV's radiative damping can be neglected [19]. Then the AUV body in waves with an effective mass of $M+m_{add}-m$ is subjected to the following forces: a waves' vertical excitation force F_e , a viscous damping force $-\lambda \dot{z}_{AUV}$, a hydrostatic spring force $-k_{AUV}z_{AUV}$, an electromagnetic damping force $c_{PTO}(\dot{z}_{AUV} - \dot{z}_{PTO})$ from the PTO, and a spring force $k_{PTO}(z_{AUV} - z_{PTO})$ from the PTO. The forces applied on the inside translator are rather simple. They include an electromagnetic damping force $c_{PTO}(\dot{z}_{PTO} - \dot{z}_{AUV})$ and a spring force $k_{PTO}(z_{PTO} - z_{AUV})$, both from the AUV body through coupling. The weight of the AUV body and the weight of the translator are pre-balanced by the buoyant force and spring force in static equilibrium, respectively. By applying the Newton's second law to the AUV body and the translator, two governing equations for the coupled AUV and PTO in heave motion can be obtained as follows:

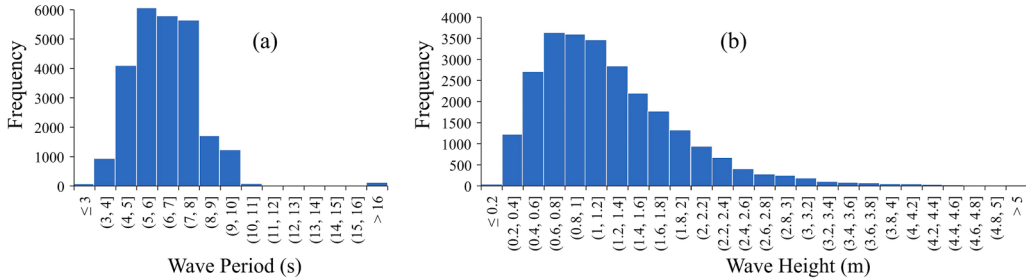


Fig. 4. Histogram of the wave period (a) and wave height (b) in the Gulf of Mexico.

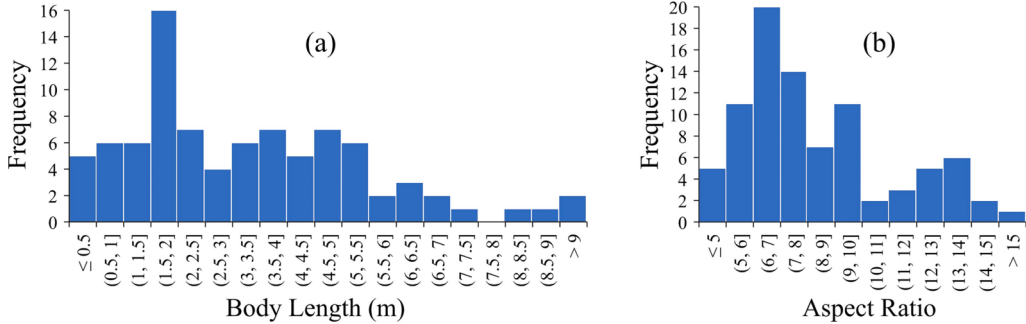


Fig. 5. Histogram of body length (a) and aspect ratio (b) of torpedo shaped AUVs.

$$(M + m_{add} - m)\ddot{z}_{AUV} + \lambda\dot{z}_{AUV} + c_{PTO}(\dot{z}_{PTO} - \dot{z}_{AUV}) + k_{AUV}z_{AUV} + k_{PTO}(z_{PTO} - z_{AUV}) = F_e, \quad (1)$$

$$m\ddot{z}_{PTO} + c_{PTO}(\dot{z}_{AUV} - \dot{z}_{PTO}) + k_{PTO}(z_{AUV} - z_{PTO}) = 0. \quad (2)$$

For two coupled mass-spring-damper subsystems in general, the coupling complicates the resonant behavior of the overall system largely [20]. To capture some key features for the present feasibility analysis, approximations are made by dealing with two separate subsystems with some simplifications. Assume that an AUV with its PTO completely locked has a heave resonant frequency f_{AUV} and an operational PTO alone has a resonant frequency f_{PTO} . Then for a coupled system of the two as in Fig. 6 to achieve the highest possible efficiency, the general resonant condition $f_{AUV} = f_{PTO} = f_w$ needs to be met. A fundamental question is that, in a practical AUV design, can such a condition ever be met?

For the first subsystem – the AUV with a locked PTO, Eq. (1) reduces to

$$a\ddot{z}_{AUV} + b\dot{z}_{AUV} + cz_{AUV} = e, \quad (3)$$

where $a = M + m_{add}$, $b = \lambda$, $c = k_{AUV}$, and $e = F_e$. For a dynamic system mathematically modelled in this form, the damped natural frequency f_n is [26]:

$$f_n = \frac{1}{2\pi} \sqrt{\frac{c}{a} - \frac{1}{4} \left(\frac{b}{a}\right)^2}. \quad (4)$$

For the AUV of Fig. 6, the hydrostatic heave stiffness is $k_{AUV} = \rho g A$, where ρ is the seawater density, g the gravitational acceleration, and A the cross-sectional area of the AUV body. When floating as in Fig. 6 with the weight and buoyant force being statically balanced, it gives $M = \rho Ad$. By further neglecting the added mass m_{add} and the viscous damping λ , the AUV's undamped heave resonant frequency f_{AUV} can be derived from Eq. (4). The final form is given as

$$f_{AUV} = \frac{1}{2\pi} \sqrt{\frac{g}{d}}. \quad (5)$$

This formula has often been used to approximately estimate the heave resonant frequency of a spar buoy [19,27]. For the AUV of Fig. 6 to have its natural heave frequency f_{AUV} matched with the dominant wave frequency of $f_w = 0.105$ Hz in Pacific waves for resonance, Eq. (5) gives a required draft to be $d \approx 22.5$ m. Note that the AUV body length L has to be greater than the draft d . Then to meet the resonance requirement, the AUV would need to have a body length over 22.5 m (e.g., 25 m or longer). Unfortunately, achieving such an overly long body length has never been of interest in practical AUV designs as evident in Fig. 5a. In other words, common AUVs can never meet the condition $f_{AUV} = f_w$ for heave resonance in the most common Pacific waves.

Alongside the challenge of matching the two frequencies f_w and f_{AUV} , the constantly changing wave frequency itself poses another challenge. In wave energy conversion in general, diverse active PTO control technologies (e.g., frequency tuning, phase control, etc.) have been investigated to broaden a reciprocating WEC's responsiveness to the changing wave frequency for the best efficiency [28]. Nonetheless, they are mostly theoretical work, and are not readily available yet for practical implementation because of some technological barriers and significantly increased complexity [17]. This is especially true for AUV applications due to the very limited space and weight allowances. Consequently, making the AUV's resonant frequency f_{AUV} tunable to match with the changing wave frequency f_w for resonance becomes impractical.

4.2. Pitch resonance

For a slender spar buoy like the partially submerged AUV in Fig. 6, it is difficult to have it maintain a vertical orientation in waves and perform heave motion only [19]. In addition to the heave motion, pitch motion could be strong as well. In fact, for an axisymmetric WEC riding waves, the theoretical maximum power absorption limit in pitch or surge motion is twice that in heave motion [29,30]. This could strongly support the idea of strengthening the AUV's pitch motion for wave energy conversion. The AUV's resonant behavior in pitch motion,

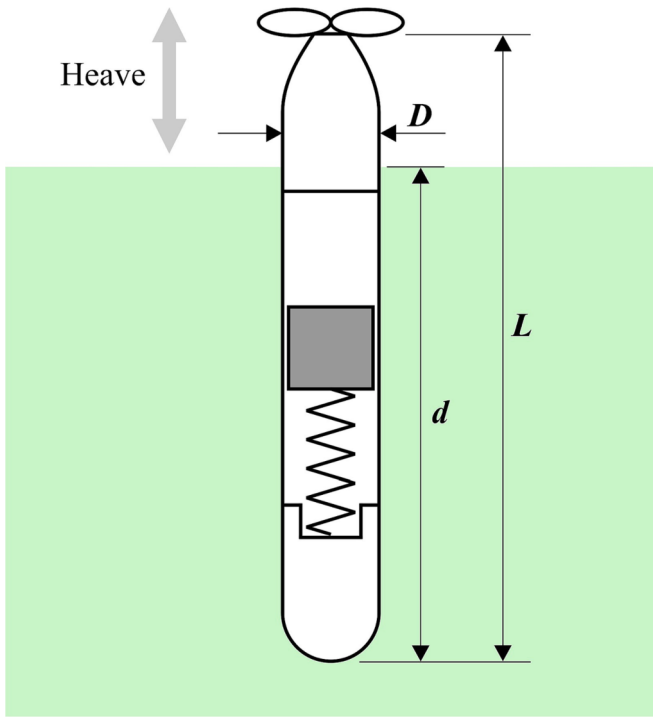


Fig. 6. Concept AUV in heave motion.

however, is more complex than that in heave motion. Besides, the interaction from the mostly unavoidable heave motion complicates the pitch motion analysis even more.

In the cruising mode of the proposed concept AUV of Fig. 1, the translator is expected to be locked close to, if not exactly at, the midpoint of the AUV body length. In AUV design in general, the center of gravity of the entire AUV should also be approximately at the midpoint when the ballast tank is appropriately filled with seawater for normal cruising. In the recharging mode with the ballast tank empty for a partial submersion, assume that the translator remains locked. This way, the AUV behavior can be examined without the PTO effect for some initial understanding. Also assume that the AUV could remain vertically oriented in calm seas as illustrated in Fig. 7a. Since the AUV is in a slender cylindrical shape with the aspect ratio σ mostly greater than 5.0 as discussed in the foregoing, as an approximation the hydrostatic stability of the vertically oriented AUV can be simply judged based on the relative position between the center of the buoyancy B and the center of gravity

G (Fig. 7). When B is above G , it defines a stable state (Fig. 7a). When B coincides with G , it results in a neutrally stable state (Fig. 7b). When B is below G , it leads to an unstable state (Fig. 7c). For pitch resonance of the AUV, it requires a stable state. With a distance s between B and G (Fig. 7a), the hydrostatic restoring stiffness c is

$$c = \frac{1}{4} \pi D^2 \rho g s. \quad (6)$$

Then with a defined mass moment of inertia I about G for the pitch motion and by neglecting the added mass moment of inertial, at a small amplitude of the pitch motion the undamped resonant frequency can be determined using [26]

$$f_\phi = \frac{1}{2\pi} \sqrt{\frac{c}{I}}. \quad (7)$$

The reality is that, in general AUV designs, making B above G as in Fig. 7a is impractical. Having the AUV of Fig. 7a (with the translator locked in the middle) remain vertically oriented in calm seas is highly unlikely either. These two points can be easily validated through some static equilibrium analyses as follows.

When the AUV is fully submerged for cruising (Fig. 7d), the ballast tank as marked in region 1 is filled with seawater of mass m_b , and the overall AUV is almost neutrally buoyant with a center of gravity approximately at the midpoint of the AUV's body length for easy maneuver and control. Region 2 in Fig. 7d is a specified region for the purpose of discussion only. It is symmetrical (very closely, if not exactly) to region 1 about the midpoint. Then by practically emptying the ballast tank in region 1 and imaginarily removing a mass m_b from region 2, the reduced AUV would remain its center of gravity at the midpoint. Consequently, a partially submerged AUV with an empty ballast tank can be modeled as the reduced AUV plus an additional mass m_b in region 2, as illustrated in Fig. 7b.

Note that in Fig. 7d, the seawater in the ballast tank is placed to the extreme trailing end (region 1) of the AUV, which makes the additional mass m_b to be placed in the extreme leading end (region 2). Then by emptying the ballast tank from the fully submerged state of Fig. 7d to achieve the partially submerged state of Fig. 7b, the yielded center of gravity G in Fig. 7b would be in its lowest possible position. By assuming a cylindrical AUV body of diameter D throughout the entire length L , analytical derivation (omitted) shows that this lowest possible center of gravity G coincide perfectly with the center of Buoyancy B (Fig. 7b), presenting a neutrally stable AUV position. As a result, the hydrostatic restoring stiffness c vanishes and the pitch resonance can never occur.

In practical AUV designs, however, the space in the extreme trailing end is always taken by some driving mechanisms for propellers and/or some other control surfaces. Therefore, the extreme mass distribution of

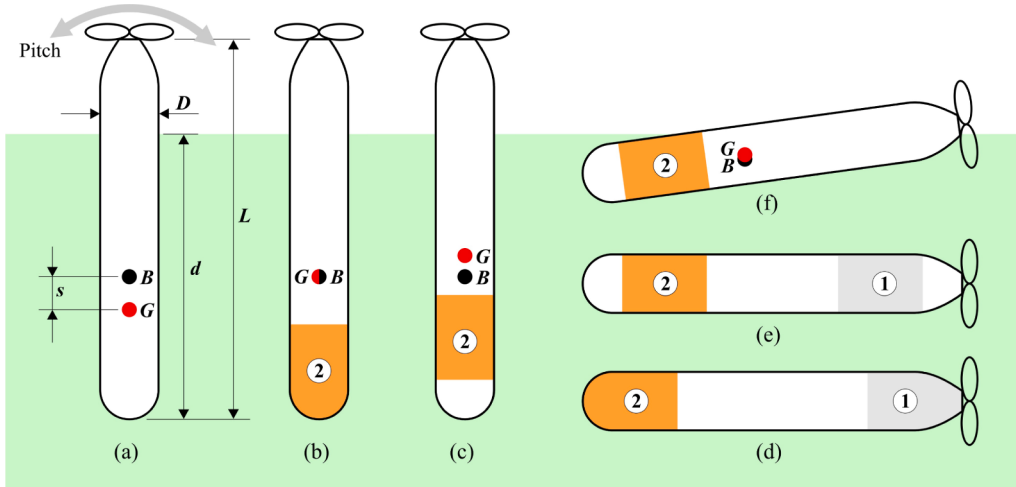


Fig. 7. Concept AUV under various conditions in calm seas. (a) Partially submerged AUV in a vertical orientation that is assumed stable. (b) Partially submerged AUV in a vertical orientation that is neutrally stable. (c) Partially submerged AUV in a vertical orientation that is unstable. (d) Fully submerged AUV with ballast water in the extreme trailing end. (e) Fully submerged AUV with ballast water somewhat away from the extreme trailing end. (f) Partially submerged AUV in a truly stable orientation.

Fig. 7d is difficult to realize, and a more realistic mass distribution of **Fig. 7e** should be adopted. The change from **Fig. 7d** to **e** is reflected on a displacement of the mass m_b away from the extreme positions in both regions 1 and 2 in a symmetrical manner about the midpoint. With such a change, when the fully submerged AUV of **Fig. 7e** has its ballast tank emptied to become the partially submerged AUV of **Fig. 7c**, the center of mass G in **Fig. 7c** would be always above the center of buoyancy B , presenting an unstable AUV position. Of course, such an unstable position cannot remain. The partially submerged AUV would quickly find a new stable position to maintain its stable equilibrium in calm seas, as illustrated in **Fig. 7f**.

In the new stable position of **Fig. 7f**, the partially submerged AUV could still have its center of gravity G above the center of buoyancy B , but the stable condition should now be based on the relative position between G and a metacenter (not shown) [31]. The AUV in this stable position regains a hydrostatic restoring stiffness, which gives it the potential for pitch resonance in waves. Nonetheless, when the AUV moves away from this stable position, the hydrostatic restoring stiffness will vanish and the AUV will become unstable again. Such an intermittent behavior makes it very difficult for the AUV to establish a strong pitch resonance.

It is noteworthy that, when the spring suspended translator inside the AUV is unlocked from the midpoint, a downward repositioning of the translator in a vertical orientation of the partially submerged AUV might be able to lower the center of mass G below the center of buoyancy B as in **Fig. 7a**. Under such a condition, the vertical orientation would become stable, and the partially submerged AUV would be able to maintain such a vertical orientation in calm seas. In waves, however, due to the continuously changing relative position between the translator and the AUV body, the stable condition for pitch resonance (i.e., G below B) may occur only momentarily in an intermittent fashion, preventing profound pitch resonance from occurring.

Overall, for a partially submerged AUV in a vertical equilibrium orientation to ride waves, no matter in heave motion, pitch motion, or a joint motion of both, it is hardly possible to achieve a profound resonance under typical wave conditions.

5. Non-resonant approach: Considerations

Incapable of resonating in typical waves poses a negative impact on the AUV design for energy harvesting. On the other hand, it could bring two advantages: (i) the AUV's performance can be much consistent in a wide range of the wave frequency and, (ii) the AUV's ballast tank can have a very small size that may leave most of the allowable mass to the PTO and payload. By giving up the resonance pursuit, there will be no need to make the AUV partially submerged in the recharging mode. Therefore, only a very small ballast tank is needed in the AUV design. When emptied for recharging, the small ballast tank could keep the AUV stay on the free surface in calm seas with the AUV body almost fully submerged. Then in waves the AUV would remain on, or very close to, the free surface without sinking into the deep sea. Note that under such an almost fully submerged condition, even if the wave riding AUV could have the heave motion only, the hydrostatic heave stiffness would vanish, making the heave resonant frequency become zero.

Based on such an almost fully submerged AUV with a vertical equilibrium orientation, and by taking the advantages as mentioned above, it becomes essential to achieve a high enough non-resonant efficiency of the AUV to meet the power demand for recharging. To demonstrate the feasibility, an analytical model based on some simplifications/assumptions has been developed. A frequency up-conversion approach has also been implemented in the AUV design of **Fig. 1**, which is reflected in the analytical model. The frequency up-conversion and the analytical model are discussed in the following.

5.1. Frequency up-conversion

For the proposed AUV of **Fig. 1** under an almost fully submerged condition with a vertical equilibrium orientation, the AUV's body motion would largely follow the water motion in waves at a dominant wave frequency with no resonance. Consider simple deep waves as an example, water particles in waves perform circular motion in a vertical plane with a horizontal Stokes drift, and the diameter of the circular motion decays exponentially with the water depth [32,33]. A series of vector fields in **Fig. 8** shows the velocity patterns of the water motion in one wave period, created using such an analytical model in absence of

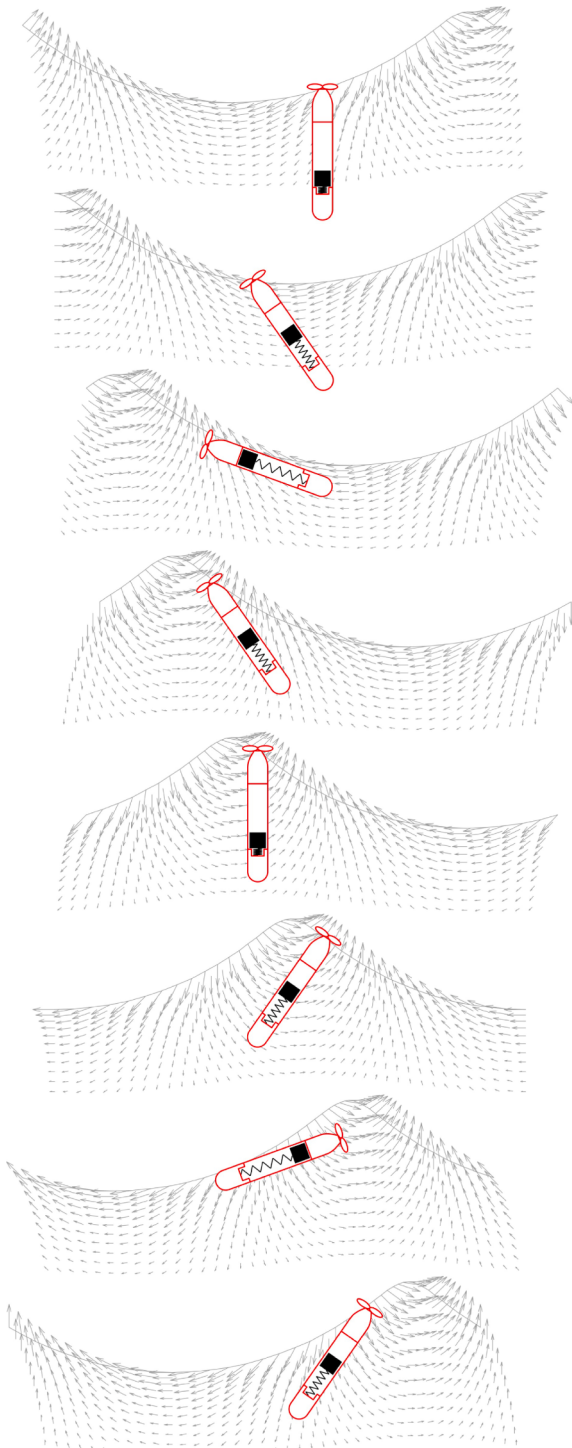


Fig. 8. An assumed AUV motion in waves.

the AUV. A possible AUV motion is also illustrated in Fig. 8 by means of superposition with the velocity fields. Due to the wave-AUV interaction coupled with the internal mass-spring-damper mechanism (i.e., the PTO), the AUV's body motion in waves could be very complex. The assumed AUV motion of Fig. 8 reflects some main motion features, which help gain preliminary understanding for further discussion. In this case, both heave and pitch motions of the AUV body are considered.

Since waves are usually at very low frequencies (e.g., $f_w = 0.105$ Hz in Pacific waves), for an AUV with its PTO translator—the sliding mass—oscillating at the same frequency would produce very limited power. This is particularly true considering the limited body length of the AUV with on resonance. To increase the efficiency, frequency up-conversion (FUC) from a low wave frequency to a higher translator oscillation frequency would be highly desirable.

FUC is a mechanism being investigated mainly for applications in sensors [34] and miniature energy harvesters [35]. It uses a low frequency excitation (e.g., human walking, wave riding, etc.) to drive some mechanical structures at higher natural frequencies (e.g., a cantilever beam) for an improved efficiency. Various FUC methods have been reported in the literature. Examples include mechanical impact [36,37], mechanical plucking [35,38], impulse-like magnetic force [39,40], and internal resonance [41]. On wave energy conversion, some FUC mechanisms have been proposed as well. For example, Du et al. [42] used vortex shedding from a bluff body to excite a piezoelectric cantilever beam for FUC in one WEC design. Chen et al. [43] employed a geared linkage mechanism to drive a piezoelectric diaphragm for FUC in another WEC design.

In the present work, the assumed AUV motion in Fig. 8 demonstrates a new FUC mechanism. Fig. 9 compares the translator's instantaneous positions relative to the AUV hull during one period of the wave motion in Fig. 8. All the instantaneous AUV body positions are presented vertically for easy comparison. Being supported by a compression spring, the translator stays low when the AUV body is in a vertical position and moves up when the AUV body leans away. Such a translator motion is caused by the change of its weight component along the AUV centerline due to leaning. Evidently, with the AUV body completing one period of motion in one period of waves, the translator fulfills two periods of oscillation along the AUV centerline, leading to a frequency doubling. Note that such a FUC mechanism happens naturally, and there is no need for active control.

For the proposed concept AUV of Fig. 1, the FUC can be further enhanced by means of mechanical impact [36,37] without increasing the system complexity. Imagine that there is no limitation in the oscillation range of the translator. Then the translator would be able to perform a full range of oscillation inside the AUV at any amplitudes without striking some sort of end stops. In practice, however, the space inside an AUV that could be allocated to the PTO unit is usually very limited, but the wave excited oscillation of the translator could have a large amplitude depending on design parameters and wave conditions. When the oscillation range of the translator is greater than its physically allowable maximum range, the translator could hit a disc spring at each

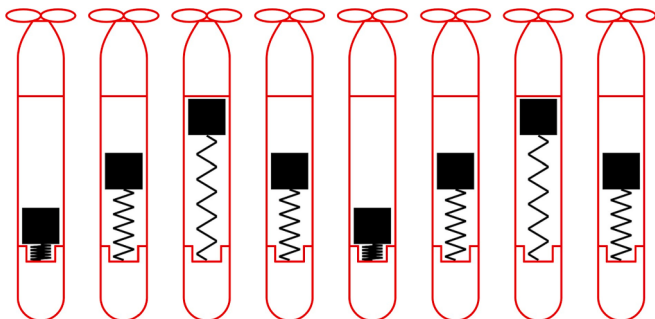


Fig. 9. Comparison of the translator's instantaneous positions in Fig. 8.

of the two ends and rebound. Such repeated rebounds would then increase the translator's oscillation frequency, leading to a further elevated FUC.

5.2. Analytical modeling

For an almost fully submerged AUV with a vertical equilibrium orientation, the AUV's body motion would involve both the heave motion and pitch motion as schematically illustrated in Fig. 8. It is expected though that the contribution from the pitch motion is much more than from the heave motion (upon design optimization) [29,30]. In analytical modeling, simple deep waves with a wave frequency f_w and wave height H are considered. Even in such simple waves, the true body motion of the AUV can be very complex. For analysis, however, the complex AUV motion can be decomposed into some simple component motions. To keep main features in the AUV motion and to avoid the complexity in dealing with wave-AUV interaction, two dominant component motions with some approximations are considered in this analysis. They are the orbital translation along a circular path of diameter H (i.e., the wave height, Fig. 10a), and the pitch motion in the form of a sinusoidal angular oscillation with a neutral position being vertical (Fig. 10b). The orbital translation is essentially a combination of heave and surge, and has a constant linear velocity $v_{AUV} = \pi f_w H$. The pitch motion is analytically expressed as $\theta_{AUV} = \theta_0 \sin(2\pi f_w t + \phi_0)$, where θ_{AUV} is the angular position, θ_0 the angular amplitude, t the time, and ϕ_0 the initial phase angle. By taking derivative of θ_{AUV} with respect to time, the angular velocity ω_{AUV} is then $\omega_{AUV} = 2\pi f_w \theta_0 \cos(2\pi f_w t + \phi_0)$.

Based on the above assumed AUV body motion in waves, the analytical modeling focuses on the translator's sliding motion inside the AUV. The translator's longitudinal position z_{PTO} with respect to the AUV hull and the maximum oscillation range $2z_0$ are defined in Fig. 10b. Note that z_{PTO} is measured from the midpoint of the range $2z_0$. When the translator moves in the range $|z_{PTO}| \leq z_0$, only the compression spring of a stiffness k_{PTO} is in contact with the translator. When $|z_{PTO}| > z_0$, however, both the compression spring and a disc spring (see Fig. 1) jointly come into effect. The spring stiffness k of the disc spring is expressed as $k = nmg/z_0$ for convenience purpose, where n is a tunable number to achieve a desired value of k . Usually, k could be one to three orders of magnitude higher than k_{PTO} .

When the AUV body is in a vertical equilibrium orientation and the inside translator is in a static equilibrium, the translator's equilibrium position along the AUV's longitudinal axis can be preset anywhere between $-z_0$ and z_0 even with a specified spring stiffness k_{PTO} and translator mass m . The variation of such a static equilibrium position can be realized by selecting springs with different natural lengths and by using the weight mg for a static compression. By referring to the midpoint of the range $2z_0$ and by introducing a variable ϵ , the static equilibrium position of the translator can be measured as ϵz_0 as shown in Fig. 10c. Note that ϵ has a value between -1 and 1. Obviously, the value selection for ϵ in optimal PTO design would largely affect the translator's oscillation in the confined range $2z_0$ and the PTO's power generation capability.

When the translator moves along the z_{PTO} -axis (Fig. 10b) with $|z_{PTO}| \leq z_0$, the forces applied on the translator along this axis include a damping force $-c_{PTO}\dot{z}_{PTO}$, a spring force $-k_{PTO}(z_{PTO} - \epsilon z_0) + mg$, and a weight component $-mg\cos(\theta_{AUV})$. On the spring force, the term mg is due to pre-compression of the spring to balance the weight mg for a static equilibrium of the translator when the AUV is in the vertical orientation. Since the z_{PTO} -axis is based on a non-inertial reference frame – the AUV body, two inertial forces also need to be accounted for. They are the two centrifugal forces due to the AUV's orbital translation and pitch motion, respectively. For the orbital translation (Fig. 10a), the centrifugal force component along the z_{PTO} -axis is $-(mv_{AUV}^2/0.5H)\cos(\phi + \theta_{AUV})$. For the pitch motion (Fig. 10b), the centrifugal force is $m\omega_{AUV}^2 z_{PTO}$, which is all along the z_{PTO} -axis. Considering all the three applied forces and two

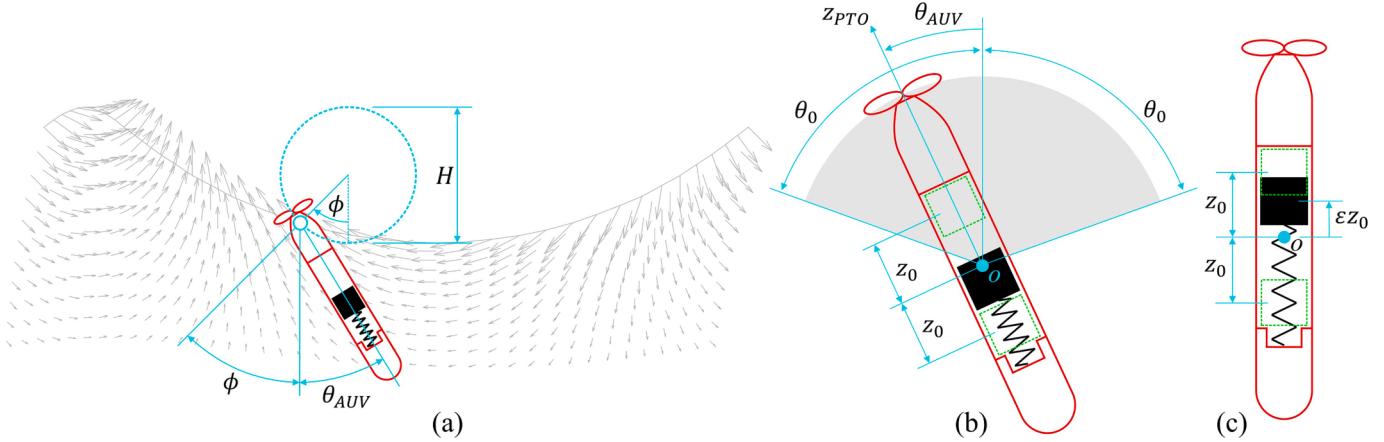


Fig. 10. Definition of certain parameters. (a) Orbital translation of the AUV. (b) Pitch motion of the AUV. (c) Static equilibrium position of the translator defined by ε ($-1 \leq \varepsilon \leq 1$).

inertial forces, applying the Newton's second law to the translator along the z_{PTO} -axis yields a governing equation as follows:

$$\begin{aligned} m\ddot{z}_{PTO} &= -c_{PTO}\dot{z}_{PTO} - k_{PTO}(z_{PTO} - \varepsilon z_0) + mg - mg\cos(\theta_{AUV}) \\ &\quad - (mv_{AUV}^2/0.5H)\cos(\phi + \theta_{AUV}) + m\omega_{AUV}^2 z_{PTO}. \end{aligned} \quad (8)$$

By applying the earlier defined v_{AUV} , θ_{AUV} , and ω_{AUV} to Eq. (8), it can be rewritten as

$$\begin{aligned} m\ddot{z}_{PTO} + c_{PTO}\dot{z}_{PTO} + (k_{PTO} - m(2\pi f_w \theta_0 \cos(2\pi f_w t + \phi_0))^2)z_{PTO} \\ = -2\pi^2 f_w^2 m H \cos(2\pi f_w t + \theta_0 \sin(2\pi f_w t + \phi_0)) \\ + (1 - \cos(\theta_0 \sin(2\pi f_w t + \phi_0)))mg + \varepsilon k_{PTO} z_0 (\text{when } |z_{PTO}| \leq z_0). \end{aligned} \quad (9)$$

When the translator travels beyond $|z_{PTO}| \leq z_0$, it will hit a disc spring with a stiffness $k = nmg/z_0$ as discussed in the forgoing and produce an additional spring force $(nmg/z_0)(z_{PTO} \mp z_0)$. Then by adding this force to the right-hand side of Eq. (8) and rewriting it, two more governing equations are obtained:

$$\begin{aligned} m\ddot{z}_{PTO} + c_{PTO}\dot{z}_{PTO} + (k_{PTO} + nmg/z_0 - m(2\pi f_w \theta_0 \cos(2\pi f_w t + \phi_0))^2)z_{PTO} \\ = -2\pi^2 f_w^2 m H \cos(2\pi f_w t + \theta_0 \sin(2\pi f_w t + \phi_0)) \\ + (1 + n - \cos(\theta_0 \sin(2\pi f_w t + \phi_0)))mg + \varepsilon k_{PTO} z_0 (\text{when } z_{PTO} > z_0); \end{aligned} \quad (10)$$

$$\begin{aligned} m\ddot{z}_{PTO} + c_{PTO}\dot{z}_{PTO} + (k_{PTO} + nmg/z_0 - m(2\pi f_w \theta_0 \cos(2\pi f_w t + \phi_0))^2)z_{PTO} \\ = -2\pi^2 f_w^2 m H \cos(2\pi f_w t + \theta_0 \sin(2\pi f_w t + \phi_0)) \\ + (1 - n - \cos(\theta_0 \sin(2\pi f_w t + \phi_0)))mg + \varepsilon k_{PTO} z_0 (\text{when } z_{PTO} < -z_0). \end{aligned} \quad (11)$$

Based on numerical solutions of the translator's displacement z_{PTO} and velocity \dot{z}_{PTO} as a function of time t from Eqs. (9) through (11), the average power \bar{P} from the PTO can be evaluated using

$$\bar{P} = \frac{c_{PTO}}{T} \int_0^T \left(\dot{z}_{PTO} \right)^2 dt, \quad (12)$$

where T is the time duration for evaluation.

6. Results and discussion

Due to the practical challenges for the resonant approach in Section 4, further exploration in this work is based on the non-resonant approach in Section 5 for the feasibility study. With a given set of values for parameters H , f_w , m , k_{PTO} , c_{PTO} , θ_0 , z_0 , ε , n , and ϕ_0 , time traces for the translator's displacement z_{PTO} and velocity \dot{z}_{PTO} can be obtained

by numerically solving Eqs. (9), (10), and (11) in Matlab using its differential equation solver ode45. Then the PTO's power generation can be evaluated use Eq. (12). In the numerical approach, initial conditions for z_{PTO} and \dot{z}_{PTO} can be roughly assigned since their effect is only limited to a short period of time in the beginning phase. For all the numerical results presented hereafter, they are based on some time traces with each being 900-second long after truncating the first 100 s.

6.1. Parameter consideration for initial characterization

In considering certain parameters for a practical AUV design, some realistic constraints are imposed. Specifically, the most common wave conditions in the Pacific Ocean and the most popular AUV parameters in existing AUV designs are employed first. They are the wave frequency of $f_w = 0.105$ Hz (Fig. 3a), the wave height of $H = 1.9$ m (Fig. 3b), the AUV body length $L = 1.75$ m (Fig. 5a), and the AUV body aspect ratio $\sigma = 6.5$ (Fig. 5b). Under such conditions, the wave power density is $P_{density} = \rho g^2 H^2 / 64\pi f_w = 16.9$ kW/m [23], and the AUV body diameter is $D = L/\sigma = 0.27$ m. To meet the neutral buoyancy requirement with an almost full submersion in seawater of a density $\rho = 1025$ kg/m³, the overall AUV mass is approximately $M = 100$ kg. Assume that no more than 50 % of the overall mass should be allocated to the translator alone, $m \leq 0.5M = 50$ kg. Also assume that no more than 80 % of the AUV body length should be used for translator's moving range $2z_0$. Then $2z_0 \leq 0.8L$ gives $z_0 \leq 0.70$ m. On presetting the static equilibrium position of the translator, ε can have a value in the range of $-1 \leq \varepsilon \leq 1$ as stated earlier. On choosing the spring stiffness of the two identical disc springs using $k = nmg/z_0$, $n = 100$ has been applied to all the numerical runs based on some initial trials. The initial phase angle ϕ_0 has an almost negligible effect on the average power \bar{P} . For this reason, $\phi_0 = 0$ has been used in all the numerical runs.

For the first peak of the AUV's power generation capability, a set of values were assigned to the following parameters in an initial numerical run: $f_w = 0.105$ Hz, $H = 1.9$ m, $m = 0.5M = 50$ kg, $z_0 = L/4 = 0.44$ m, $\varepsilon = -1$, $\phi_0 = 0$, $n = 100$, and $\theta_0 = \pi/3$. The average power \bar{P} was then obtained under varied k_{PTO} and c_{PTO} , as shown in Fig. 11. In this case, the maximum power of $\bar{P}_{max} = 30.1$ W is achieved at $k_{PTO} = 240$ N/m and $c_{PTO} = 180$ kg/s. The corresponding time trace of z_{PTO} at this peak point and more time traces at some other specified values of k_{PTO} and c_{PTO} are presented in Fig. 12. Evidently, for all the combined values of k_{PTO} and c_{PTO} in the entire examined range, the dominant oscillation frequency of the translator always equals two times of the wave frequency f_w . This conclusion validates the FUC approach for frequency doubling, as discussed in Section 5.1.

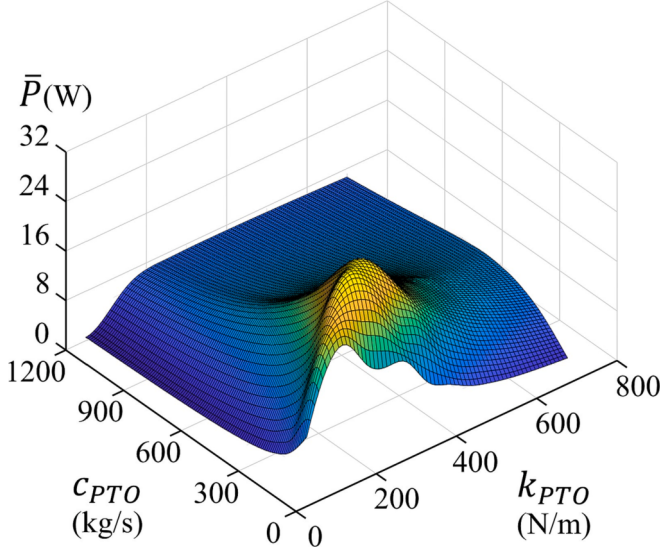


Fig. 11. \bar{P} as a function of k_{PTO} and c_{PTO} . The other parameters are $f_W = 0.105$ Hz, $H = 1.9$ m, $m = 50$ kg, $z_0 = 0.44$ m, $\varepsilon = -1$, $\phi_0 = 0$, $n = 100$, and $\theta_0 = \pi/3$.

6.2. Effect of design parameters ε , z_0 , and m on power generation

After the above initial run, the effect of ε is examined first for an optimal AUV design. By systematically changing the value of ε in the range of $-1 \leq \varepsilon \leq 1$ and by keeping all the other parameters unchanged from the initial run, a series of graphs similar to Fig. 11 have been produced. Then the maximum value of \bar{P}_{max} is identified from each graph. Fig. 13 presents such numerical results to reflect the $\bar{P}_{max} \varepsilon$ relation. A general observation is that \bar{P}_{max} monotonously decrease with increased ε . Therefore, the AUV can produce the highest power at $\varepsilon = -1$. Note that $\varepsilon = -1$ defines the lowest possible static equilibrium position of the translator in its allowable moving range $\pm z_0$ when the AUV is vertically oriented.

Following the same approach as above, the effects of z_0 and m are examined next. In one case, z_0 is changed in the range of $0 \leq z_0 \leq 0.7$ m, and all the other parameters are fixed at the same values as in the initial run (including $\varepsilon = -1$ and $m = 50$ kg). In another case, m is altered in the range of $0 \leq m \leq 50$ kg, and the other parameters are still fixed at the same values as in the initial run (including $\varepsilon = -1$ and $z_0 =$

0.44 m). As shown in Fig. 14, a higher value of z_0 promises a higher capability in power generation. Similarly, a larger translator mass can produce more power as depicted in Fig. 15.

Jointly considering these parametric effects, a general principle to guide the AUV design can be drawn. It is to allocate as much of mass (m) and sliding space ($2z_0$ and ε) of the translator as possible for the best power generation capability. Following this principle and considering some realistic constraints in the present feasibility study, $m/M = 0.5$, $(2z_0)/L = 0.5$, and $\varepsilon = -1$ are adopted for all the numerical runs to be

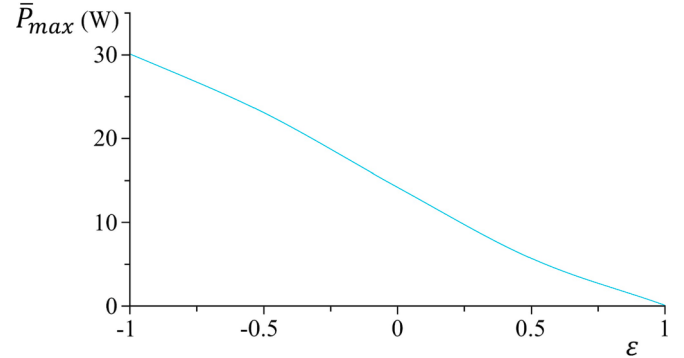


Fig. 13. \bar{P}_{max} as a function of ε . All the other parameters are the same as in Fig. 11.

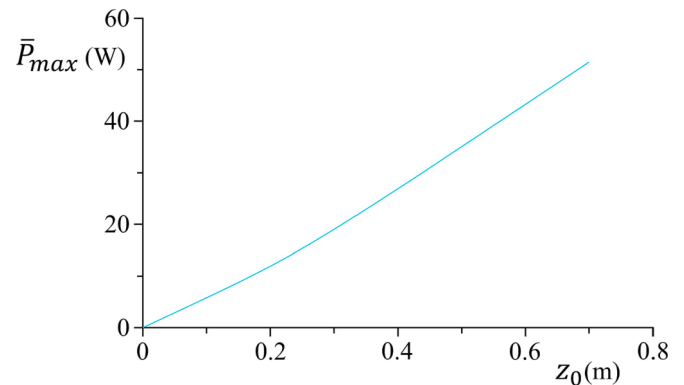


Fig. 14. \bar{P}_{max} as a function of z_0 . All the other parameters are the same as in Fig. 11.

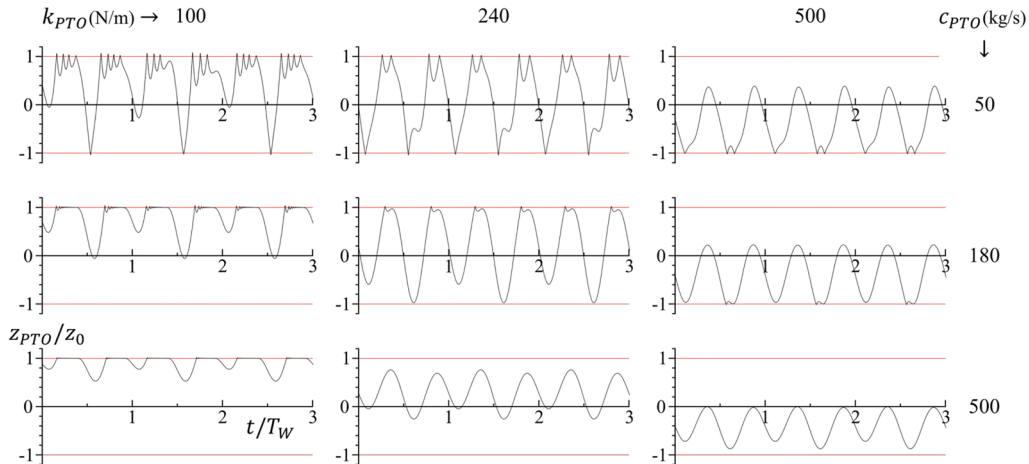


Fig. 12. Typical time traces of the translator's displacement associated with Fig. 11. The corresponding values of k_{PTO} and c_{PTO} are provided on the top row and the right column, respectively. The displacement z_{PTO} is normalized by z_0 , and the time t is normalized by the wave period $T_W (= 1/f_W)$. The two red lines in each time trace define the border for rebounds. (For interpretation of the references to colour in this figure legend, the reader is referred to the web version of this article.)

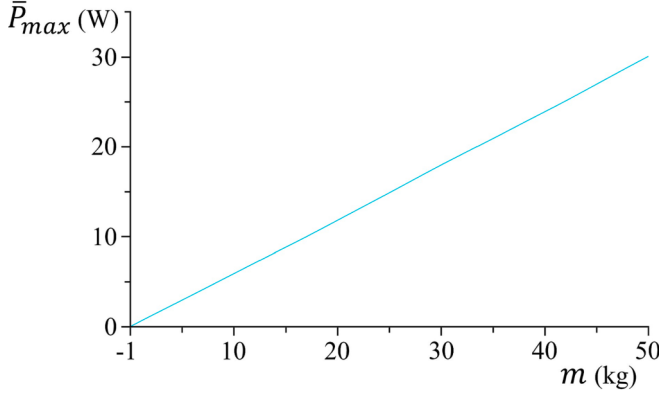


Fig. 15. \bar{P}_{\max} as a function of m . All the other parameters are the same as in Fig. 11.

discussed hereafter. Such a parameter selection would still leave a 50 % of the AUV mass M and a 50 % of the AUV body length L for other necessary AUV components (Fig. 1).

6.3. Effect of rebounds on power generation

As a part of the FUC effect in addition to the frequency doubling, rebounds at the ends of the sliding range due to the mechanical impact contributes to the power generation. Referring to the typical time traces of Fig. 12 that are associated with the initial run as reflected in Fig. 11, rebounds only occur in certain combinations of k_{PTO} and c_{PTO} , particularly in the lower range of c_{PTO} . Figs. 16 and 17 show the translator's sliding range normalized by z_0 as a function of k_{PTO} at $c_{PTO} = 180$ kg/s and as a function of c_{PTO} at $k_{PTO} = 240$ N/m, respectively. Note that the combination $k_{PTO} = 240$ N/m and $c_{PTO} = 180$ kg/s yields the maximum power. The two figures compare the sliding range (the shaded area in between the two blue lines) with the allocated range (the space in between the two red lines). The sliding range is defined by the highest and lowest values of z_{PTO} from individual time traces. The portions of the shaded area beyond the two red lines indicate occurrence of rebounds.

By examining the time traces of Fig. 12 with a particular focus on rebounds, a general impression is that the translator's rebounds (if occurs) are much weaker than its dominant oscillation at $2f_w$. Consequently, the power gain from rebounds is very limited. The rebounds can

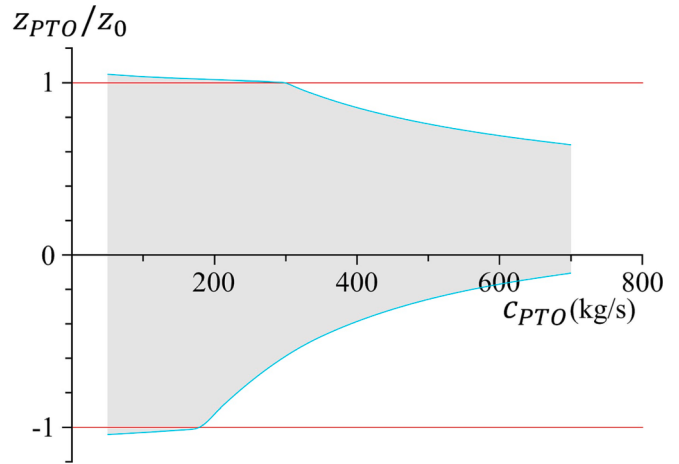


Fig. 17. The translator's normalized sliding range—the shaded area between the two blue curves—as a function of c_{PTO} at a fixed $k_{PTO} = 240$ N/m. All the other parameters are the same as in Fig. 11. The two red lines define the border for rebounds. (For interpretation of the references to colour in this figure legend, the reader is referred to the web version of this article.)

be enhanced though at low values of k_{PTO} and c_{PTO} (e.g., the top-left time trace of Fig. 12), but the overall power would then become low as well due to the low c_{PTO} . To quantify the contribution of rebounds to the power generation in Fig. 11, a model with rebounds suppressed (e.g., by assuming plastic impact) is used as a reference and compared to the present model with rebounds promoted (i.e., by employing elastic impact as in Eqs. (10) and (11)). Figs. 18 and 19 are associated with Figs. 16 and 17, respectively. They reflect the power difference between the two models under specified conditions of k_{PTO} and c_{PTO} . Evidently, some noticeable but small difference exists in a lower region in the k_{PTO} c_{PTO} domain. The difference becomes negligibly small or completely vanishes beyond the lower region. Further examination shows that, by varying the value of n in a large range to alter the disc springs' stiffness $k = nmg/z_0$, no significant change in the power gain due to rebounds has ever been observed (results not shown).

Based on the above discussion, the rebounds from mechanical impact for FUC generally does not contribute much to the AUV's capability in wave energy conversion.

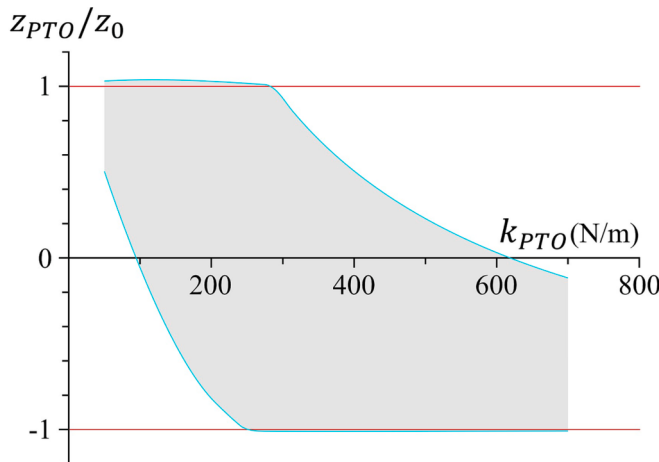


Fig. 16. The translator's normalized sliding range—the shaded area between the two blue curves—as a function of k_{PTO} at a fixed $c_{PTO} = 180$ kg/s. All the other parameters are the same as in Fig. 11. The two red lines define the border for rebounds. (For interpretation of the references to colour in this figure legend, the reader is referred to the web version of this article.)

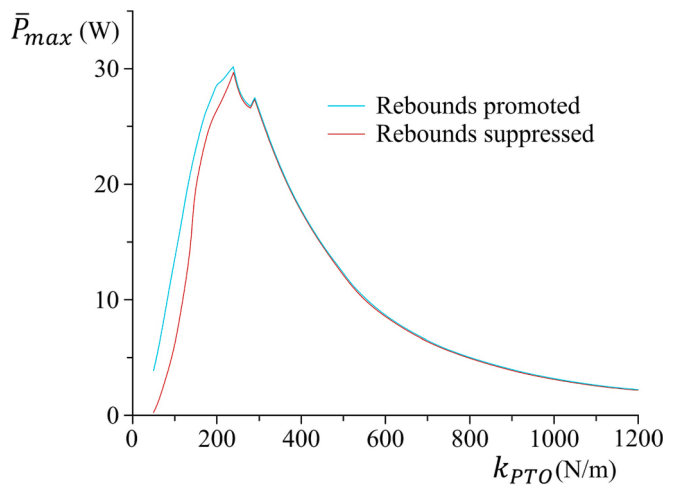


Fig. 18. Power comparison between the models with and without rebounds under the specified conditions as in Fig. 16.

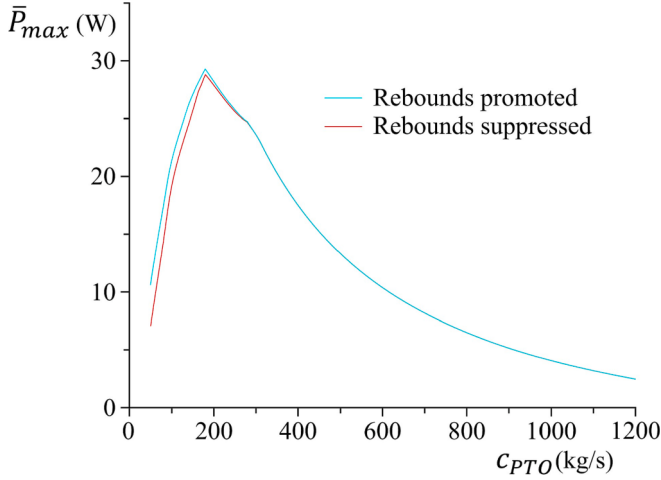


Fig. 19. Power comparison between the models with and without rebounds under the specified conditions as in Fig. 17.

6.4. Effect of wave frequency on power generation

To characterize the wave frequency effect, the value of f_W is varied in the range of $0.05 \text{ Hz} \leq f_W \leq 0.34 \text{ Hz}$, and all the other parameters are remained the same as in the initial run. No higher frequency is considered herein since wave breaking would occur at the specified wave height of $H = 1.9 \text{ m}$ [44]. By following the same approach as before to identify the maximum power \bar{P}_{max} in the k_{PTO} c_{PTO} domain for each given value of f_W , the obtained \bar{P}_{max} f_W relation is shown in Fig. 20. The curve fitting $\bar{P}_{max} = 800f_W^{1.5}$ with an R-squared of 99 % indicates a simple and clear relation: the AUV's power generation capability is proportional to the wave frequency to the power of 1.5, $\bar{P}_{max} \propto f_W^{1.5}$. This relation contrasts the one between the wave power density and the wave frequency, $P_{density} \propto f_W^{-1}$ [23].

6.5. Case study

In this case study, the most common AUV body length $L = 1.75 \text{ m}$ (Fig. 5a) and aspect ratio $\sigma = 6.5$ (Fig. 5b) are adopted. The corresponding AUV mass is $M = 100 \text{ kg}$. Following the guiding principles established in Section 6.2 with incorporation of certain realistic constraints, some fixed AUV parameters are as follows: $m = M/2 = 50 \text{ kg}$, $z_0 = L/4 = 0.44 \text{ m}$, $\varepsilon = -1$ and $n = 100$. Two representative wave conditions are considered for comparison. One is the dominant wave frequency $f_W = 0.105 \text{ Hz}$ (Fig. 3a) and wave height $H = 1.9 \text{ m}$ (Fig. 3b) in the Pacific Ocean. The other is the dominant wave frequency $f_W = 0.154 \text{ Hz}$ (Fig. 4a) and wave height $H = 0.9 \text{ m}$ (Fig. 4b) in the Gulf of Mexico. The corresponding wave power densities are 16.9 kW/m and

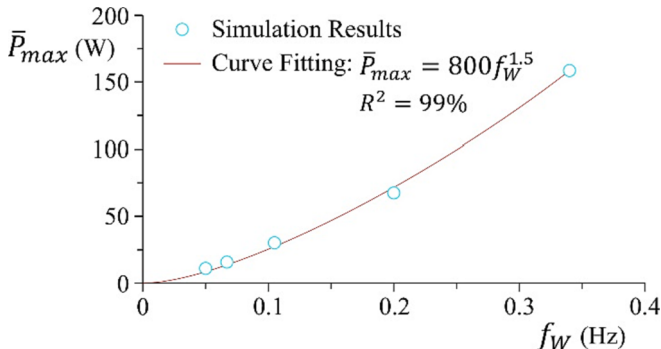


Fig. 20. \bar{P}_{max} as a function of f_W . All the other parameters are the same as in Fig. 11.

2.6 kW/m , respectively. Under each wave condition, a set of values for θ_0 are examined in the range $0 < \theta_0 \leq \pi/2$. Then at each value of θ_0 , the average power \bar{P} is computed in the k_{PTO} c_{PTO} domain.

Fig. 21 shows some typical patterns of \bar{P} in the k_{PTO} c_{PTO} domain at some specified values of θ_0 . The left column is for the AUV in Pacific waves and the right column in Gulf waves. Fig. 22 further compares \bar{P}_{max} as a function of θ_0 in Pacific and Gulf waves. Undoubtedly, the AUV's power generation capability increases with increasing θ_0 in both wave conditions. It is noteworthy that, at a specified value of θ_0 , the AUV can generate more power in relatively weak Gulf waves ($P_{density} = 2.6 \text{ kW/m}$) than in relatively strong Pacific waves ($P_{density} = 16.9 \text{ kW/m}$). Using $\theta_0 = \pi/3$ as an example, the AUV's power generation capability is $\bar{P}_{max} = 48.8 \text{ W}$ in Gulf waves, which is in comparison with $\bar{P}_{max} = 30.1 \text{ W}$ in Pacific waves. Such a seemingly counterintuitive result can be easily explained using the relation established in Section 6.4: $\bar{P}_{max} \propto f_W^{1.5}$.

A general impression from Figs. 21 and 22 is that this AUV's power generation capability is somewhat limited. The highest possible power in the examined parameter ranges is $\bar{P}_{max} = 92.1 \text{ W}$, which occurs at $\theta_0 = \pi/2$ in Gulf waves. For most existing AUVs of a body length close to 1.75 m (e.g., $1.5 \text{ m} \leq L \leq 2.0 \text{ m}$), a rechargeable battery employed would most likely have a power capacity in the range of 1.0 kWh to 2.0 kWh [2]. With a power feed below 100 W as in the cases considered herein, the battery's recharging time would go beyond 10 h . To increase an AUV's power generation capability for a reduced recharging time, a longer body length might be preferred.

As an example of a lengthened body length, a well-known unmanned underwater vehicle Bluefin-21 [45] is directly modelled. It has a body length $L = 4.938 \text{ m}$, a body diameter $D = 0.533 \text{ m}$, and a total mass $M = 750 \text{ kg}$. Accordingly, the following vehicle parameters are used in

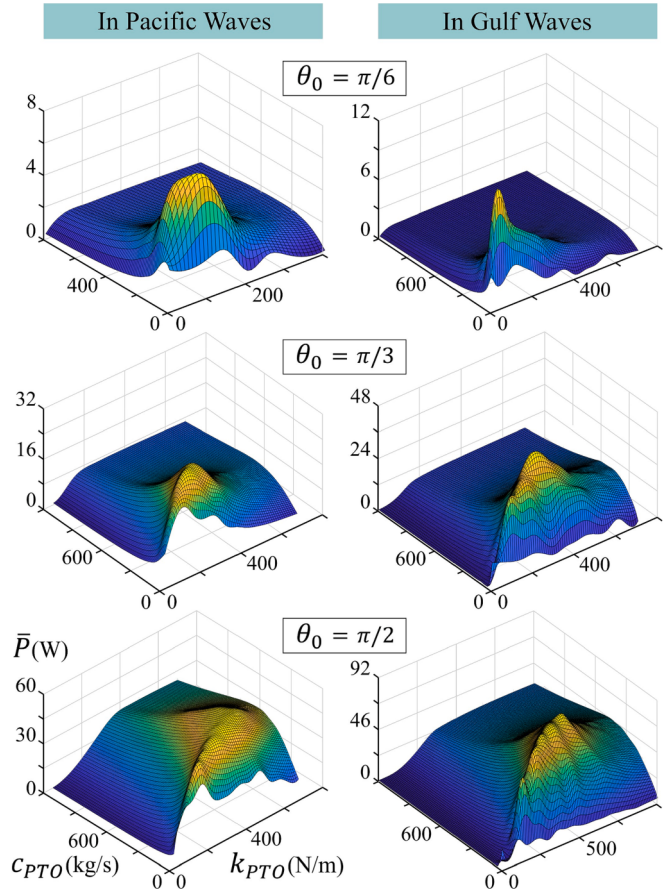


Fig. 21. Comparison of \bar{P} as a function of k_{PTO} and c_{PTO} among different values of θ_0 and between two representative wave conditions.

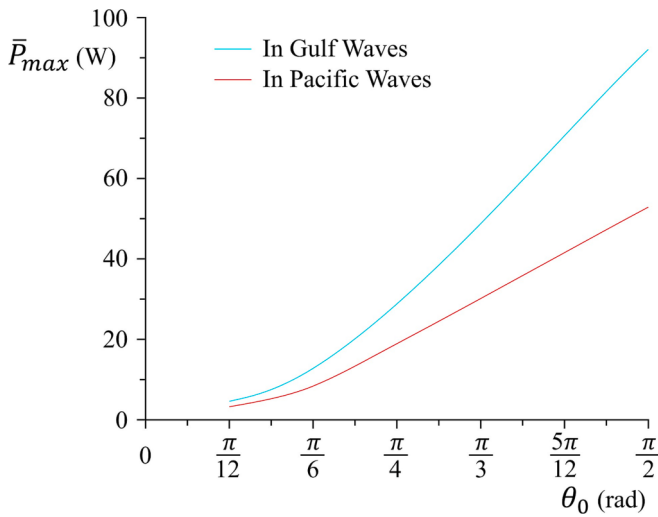


Fig. 22. Comparison of \bar{P}_{max} as a function of θ_0 between two representative wave conditions. The two curves in this figure are correlated to the two columns in Fig. 21.

simulation: $m = M/2 = 375$ kg, $z_0 = L/4 = 1.23$ m, $\varepsilon = -1$ and $n = 100$. Assume that this vehicle is exposed in Pacific waves with $f_w = 0.105$ Hz and $H = 1.9$ m. Also assume that it can achieve an angular oscillation amplitude of $\theta_0 = \pi/3$ in such waves. The simulated power pattern in the k_{PTO} c_{PTO} domain is presented in Fig. 23. It demonstrates a maximum power generation capability of $\bar{P}_{max} = 730$ W, which occurs at $k_{PTO} = 760$ N/m and $c_{PTO} = 660$ kg/s. This modelled power generation capability of Bluefin-21 ($L = 4.938$ m, $\bar{P}_{max} = 730$ W) is about 24 times higher than that of the earlier AUV under the same conditions ($L = 1.75$ m, $\bar{P}_{max} = 30.1$ W). Such a power capacity also results in a capture width ratio of 8 %. This ratio is at the low end if compared with well-developed utility scale WECs [46], so it has much room to go higher.

In all the above cases considered in this case study, further analysis indicates that an AUV body's pitch motion plays the major role in power generation from waves, whereas the heave motion plays a rather minor role (results not shown). Therefore, enhancing the AUV body's pitch motion in waves becomes critical in achieving a high capture width ratio. In a practical AUV design where mooring is prohibited, various means can help enhance the pitch motion. For example, in the recharging mode of the AUV, its tail that includes a propeller and some fins/rudders would be in the close proximity of the free surface and experience a strong lateral force in waves. In contrast, the smooth nose and midbody underneath the free surface would experience a much milder lateral force. The joint effect would then enable a strong pitch motion of the AUV. Another approach to further enhance the pitch motion would be to appropriately position the moving range of the sliding mass inside the AUV. Specifically, the changing center of mass of the whole AUV should be below the center of buoyancy for stability, but the two centers should also stay close enough to assure a weak stability for an easy pitch motion (as in Section 4.2).

7. Conclusions

Feasibility study on a wave powered AUV in a torpedo shape is conducted in this work. The AUV employs a fully hull-encapsulated mass-spring-damper system as its PTO for wave energy conversion to recharge an onboard battery pack. Typical wave conditions and common AUV sizes are considered in modelling. Major research findings are summarized in the following:

- Due to the relatively small sizes of common AUVs and their almost neutrally buoyant requirement when fully submerged, it becomes

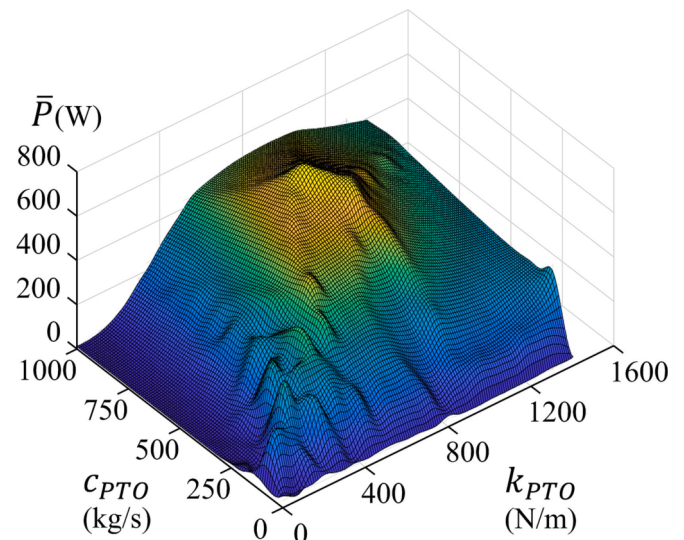


Fig. 23. \bar{P} as a function of k_{PTO} and c_{PTO} for a modelled Bluefin-21 [45] in Pacific waves at $\theta_0 = \pi/3$.

impractical to utilize the generally very low wave frequency to excite resonances for a high capture width ratio.

- By giving up the resonance pursuit but enhancing the AUV response in a wide range of the wave frequency, the proposed concept AUV can still harvest the wave power at a decently high level upon optimization, and its power generation capability is proportional to the wave frequency to the power of 1.5.
- The proposed concept AUV results in frequency doubling of its PTO's sliding mass when riding waves, which is in favor of an efficient wave energy conversion. Rebounds of the sliding mass at the two stroke ends for FUC, on the other hand, have very limited contribution in increasing the AUV's power generation capability.
- The body length of the proposed concept AUV has a strong effect on the AUV's power generation capability. The longer the body length (within a reasonable range), the more capable the AUV can harvest power from waves.
- In design of an AUV with a specified body length and total mass, it would help achieve the highest possible power generation capability of the AUV if as much mass and length as possible could be allocated to the sliding mass and its sliding range.

CRediT authorship contribution statement

Yingchen Yang: Conceptualization, Methodology, Formal analysis, Investigation, Writing – original draft, Visualization, Supervision. **Erick Martinez:** Software, Validation, Investigation, Data curation, Visualization.

Declaration of Competing Interest

The authors declare that they have no known competing financial interests or personal relationships that could have appeared to influence the work reported in this paper.

Data availability

Data will be made available on request.

Acknowledgements

The authors gratefully acknowledge Gregory Hubbard for producing some numerical solutions. This research did not receive any specific

grant from funding agencies in the public, commercial, or not-for-profit sectors.

References

- [1] Aguirre F, Vargas S, Valdes D, Tornero J. State of the art of parameters for mechanical design of an autonomous underwater vehicle. *Int J Ocean Oceanogr* 2017;11:89–113.
- [2] Autonomous Undersea Vehicle Application Center. <https://auvac.org/explore-database>. [Accessed 18 May 2022].
- [3] Townsend NC, Shenoi RA. Feasibility study of a new energy scavenging system for an autonomous underwater vehicle. *Auton Robots* 2016;40(6):973–85.
- [4] Tian B, Yu J. Current status and prospects of marine renewable energy applied in ocean robots. *Int J Energy Res* 2019;43(6):2016–31.
- [5] Crimmins D, Patty C, Beliard M, Baker J, Jalbert J, Komerska R, et al. Long-endurance test results of the solar-powered AUV system. In: OCEANS 2006, IEEE, 2006.
- [6] Chao Y. Autonomous underwater vehicles and sensors powered by ocean thermal energy. In: OCEANS 2016, IEEE, 2016.
- [7] Wang G, Yang Y, Wang S, Zhang H, Wang Y. Efficiency analysis and experimental validation of the ocean thermal energy conversion with phase change material for underwater vehicle. *Appl Energy* 2019;248:475–88.
- [8] Townsend ZC. In situ results from a new energy scavenging system for an autonomous underwater vehicle. In: OCEANS 2016, IEEE, 2016.
- [9] Zhang Y, Yang F, Li Y, Qiu W. Design and numerical investigation of a multi-directional energy-harvesting device for UUVs. *Energy* 2021;214:118978.
- [10] Ding W, Song B, Mao Z, Wang K. Experimental investigation on an ocean kinetic energy harvester for underwater gliders. In: 2015 IEEE Energy Conversion Congress and Exposition (ECCE); 2015. <https://doi.org/10.1109/ecce.2015.7309802>.
- [11] Ocean Aero. <https://oceanaeaero.com/technology>. [Accessed 18 May 2022].
- [12] Manley J, Willcox S. The wave glider: a new concept for deploying ocean instrumentation. *IEEE Instrum Meas Mag* 2010;13(6):8–13.
- [13] Shadman M, Silva C, Faller D, Wu Z, Assad LP, Landau L, et al. Ocean renewable energy potential, technology and deployments: a case study of Brazil. *Energies* 2019;12:3658.
- [14] Mwasilu F, Jung J-W. Potential for power generation from ocean wave renewable energy source: a comprehensive review on state-of-the-art technology and future prospects. *IET Renew Power Gener* 2019;13(3):363–75.
- [15] Donelan MA, Drennan WM, Katsaros KB. The air-sea momentum flux in conditions of wind sea and swell. *J Phys Oceanogr* 1997;27(10):2087–99.
- [16] Falcao AFO. Waven energy utilization: A review of the technologies. *Renew Sustain Energy Rev* 2010;14:899–918.
- [17] Sheng W. Wave energy conversion and hydrodynamics modelling technologies: a review. *Renew Sustain Energy Rev* 2019;109:482–98.
- [18] Shami EA, Zhang R, Wang X. Point absorber wave energy harvesters: a review of recent developments. *Energies* 2019;12:47.
- [19] Grilli A, Merrill J, Grilli S, Spaulding M, Cheung J. Experimental and Numerical Study of Spar Buoy-magnet/spring Oscillators used as Wave Energy Absorbers. Proceedings of the 17th International Society of Offshore and Polar Engineers (ISOPE-07). Lisbon, Portugal, July 1–6, pp. 489–496, 2007.
- [20] Chen Z, Zhou B, Zhang L, Sun L, Zhang X. Performance evaluation of a dual resonance wave-energy convertor in irregular waves. *Appl Ocean Res* 2018;77:78–88.
- [21] Gao Y, Shao S, Zou H, Tang M, Xu H, Tian C. A fully floating system for a wave energy converter with direct-driven linear generator. *Energy* 2016;95:99–109.
- [22] National Oceanic and Atmospheric Administration's National Data Buoy Center. <https://www.ndbc.noaa.gov/>. [Accessed 18 May 2022].
- [23] Falnes J. A review of wave-energy extraction. *Mar Struct* 2007;20(4):185–201.
- [24] MacCready T, Paulos J, Zambrano T. Targeting the wave resource from the power take-off perspective. Proceedings of the ASME 2012 31st International Conference on Ocean, Offshore and Arctic Engineering (OMAE2012), Rio de Janeiro, Brazil, June 10–15, 2012.
- [25] Ocean Power Technologies. <https://oceangepowertechnologies.com/pb3-powerbuoy/>. [Accessed 18 May 2022].
- [26] Faizal M, Ahmed MR, Lee Y-H. A design outline for floating point absorber wave energy converters. *Adv Mech Eng* 2014;6:846097.
- [27] Kweon H-M, Cho H-Y, Cho II-H. A study of the optimum draft of multiple resonance power buoys for maximizing electric power production. *Int J Archit Ocean Eng* 2014;6(4):813–25.
- [28] Ozkop E, Altas IH. Control, power and electrical components in wave energy conversion systems: a review of the technologies. *Renew Sustain Energy Rev* 2017;67:106–15.
- [29] Evans DV. A theory for wave-power absorption by oscillating bodies. *J Fluid Mech* 1976;77(1):1–25.
- [30] Falnes J. Optimum control of oscillation of wave-energy converters. *Int J Offshore Polar Eng* 2002;12:147–54.
- [31] White FM. Fluid mechanics. 8th ed. New York: McGraw-Hill Education; 2016.
- [32] Pickard GL, Pond S. Introductory dynamical oceanography. Oxford: Elsevier Butterworth-Heinemann; 1983.
- [33] Phillips OM. The dynamics of the upper ocean. Cambridge: Cambridge University Press; 1977.
- [34] Rodgers PW. Sub-resonant response of a mechanical system parametrically excited at its resonant frequency. *Nature* 1965;207:853.
- [35] Kathpalia B, Tan D, Stern I, Erturk A. An experimentally validated model for geometrically nonlinear plucking-based frequency-up conversion in energy harvesting. *Smart Mater Struct* 2018;27(1):015024.
- [36] Liu H, Lee C, Kobayashi T, Tay CJ, Quan C. Investigation of a MEMS piezoelectric energy harvester system with a frequency-widened-bandwidth mechanism introduced by mechanical stoppers. *Smart Mater Struct* 2012;21:35005.
- [37] Edwards B, Aw KC, Hu AP. Mechanical frequency up-conversion for sub-resonance, low-frequency vibration harvesting. *J Intell Mater Syst Struct* 2016;27(16):2145–59.
- [38] Pozzi M, Zhu M. Plucked piezoelectric bimorphs for knee-joint energy harvesting: modelling and experimental validation. *Smart Mater Struct* 2011;20:55007.
- [39] Wickensheiser AM, Garcia E. Broadband vibration-based energy harvesting improvement through frequency up-conversion by magnetic excitation. *Smart Mater Struct* 2010;19:65020.
- [40] Tang L, Yang Y, Soh C-K. Improving functionality of vibration energy harvesters using magnets. *J Intell Mater Syst Struct* 2012;23(13):1433–49.
- [41] Wu Y, Ji H, Qiu J, Liu W, Zhao J. An internal resonance based frequency up-converting energy harvester. *J Intell Mater Syst Struct* 2018;29(13):2766–81.
- [42] Du X, Zhao Y, Liu G, Zhang M, Wang Y, Yu H. Enhancement of the piezoelectric cantilever beam performance via vortex-induced vibration to harvest ocean wave energy. *Shock Vib* 2020;2020:1–11.
- [43] Chen SE, Yang R-Y, Wu G-K, Wu C-C. A piezoelectric wave-energy converter equipped with a geared-linkage-based frequency up-conversion mechanism. *Sensors* 2021;21:204.
- [44] Trujillo AP, Thurman HV. Essentials of oceanography. 13th Ed. Pearson; 2019.
- [45] General Dynamics Mission Systems, Bluefin-21 Unmanned Underwater Vehicle. <https://gdmissionsystems.com/products/underwater-vehicles/bluefin-21-autonomous-underwater-vehicle>. [Accessed 18 May 2022].
- [46] Babarit A. A database of capture width ratio of wave energy converters. *Renew Energy* 2015;80:610–28.